CHEMISTRY
A European Journal

A Journal of
ChemPubSoc Europe

Accepted Article

Title: Low and high molecular mass dithienopyrrole-naphthalene bisimide donor-acceptor compounds: synthesis, electrochemical and spectroelectrochemical behaviour

Authors: Renata Rybakiewicz, Eric Daniel Glowacki, Lukasz Skorka, Sandra Pluczyk, Pawel Zassowski, Dogukan Apaydin, Mieczyslaw Lapkowski, Malgorzata Zagorska, and Adam Pron

To be cited as: *Chem. Eur. J.* 10.1002/chem.201604672

Link to VoR: http://dx.doi.org/10.1002/chem.201604672

Supported by
ACES

WILEY-VCH

Low and high molecular mass dithienopyrrole-naphthalene bisimide donor-acceptor compounds: synthesis, electrochemical and spectroelectrochemical behaviour

Renata Rybakiewicz,*[a,b] Eric D. Glowacki,*[c] Lukasz Skorka,[b] Sandra Pluczyk,[d] Pawel Zassowski,[d] Dogukan Hazar Apaydin,[e] Mieczyslaw Lapkowski,[d,f] Malgorzata Zagorska,[b] Adam Pron*[b]

Abstract: Two low molecular weight electroactive donor-acceptor-donor (DAD) type molecules are reported, namely naphthalene bisimide symmetrically core-functionalized with dithienopyrrole (**NBI-(DTP)$_2$**) and an asymmetric core-functionalized naphthalene bisimide with dithienopyrrole substituent on one side and 2-ethylhexylamine on the other side (**NBI-DTP-NHEtHex**). Both compounds are characterized by low optical band gaps (1.52 eV and 1.65 eV, respectively). **NBI-(DTP)$_2$** undergoes oxidative electropolymerization giving the electroactive polymer of ambipolar character. Its two-step reversible reduction and oxidation is corroborated by complementary EPR and UV-vis-NIR spectroelectrochemical investigations. The polymer turned out to be electrochemically active not only in aprotic solvents but also in aqueous electrolytes, showing a distinct photocathodic current attributed to proton reduction. Additionally, **poly(NBI-(DTP)$_2$)** was successfully tested as a photodiode material.

Introduction

Organic electroactive compounds are a subject of increasing research interest over nearly three decades, following initial reports on organic light emitting diodes,[1] organic field effect transistors[2] and bulk heterojunction-type photovoltaic cells.[3] Conjugated molecules (macromolecules) consisting of alternating donor and acceptor units attract particular interest since their properties can be tuned over a wide range by strengthening or weakening donor-acceptor interactions between constitutive segments of the macromolecule through selection of appropriate groups being in conjugation.[4]

Arylene bisimides are popular electron-accepting moieties used as building blocks in (donor-acceptor) DA-type molecules and macromolecules.[5] Their core-functionalization with electron-donating groups like triphenylamine, for example, leads to significant changes in their electronic structure and can transform these normally n-type organic semiconductors into semiconductors of ambipolar character.[6] Other electron donors suitable for core functionalization of arylene bisimides involve carbazolyl groups[7] (including substituents with aromatic ring of carbazole fused with the bisimide core)[8] and alkoxy substituents.[9]

Core functionalization with thiophene derivatives constitutes another way to prepare arylene bisimide-based DA compounds. Core-substituted derivatives with thiophene,[10] ethylenedioxythiopene[11] oligothiophenes (including fused ones like thienoacenes[12] as well as annulated thiophene, *i.e.* thiophene ring being integrated to the bisimide core[13] were synthesized. These compounds can be used as substrates in the preparation of conjugated copolymers in which bisimide units alternate with oligothiophene ones.[4d] Coupling of D-A units involves Stille coupling,[14] direct arylation[10] or electrochemical oxidative polymerization.[11]

Alternating copolymers of arylene bisimides with thienoacenes[14c] are promising materials because replacing $\alpha-\alpha'$ coupled thiophenes with fused rings stiffens the macromolecule and facilitates π-stacking, leading in turn, to improved supramolecular organization. However, thienoacenes like dithienothiophene, for example, are rather weak donors. It is known that replacing the dithienothiophene unit by a dithienopyrrole increases donor acceptor interactions which leads to lowering of the ionization potential (IP) and narrowing of the band gap[15] both in alternating copolymers[16] and in low molecular weight compounds.[17] These effects make dithienopyrrole-arylene bisimide semiconductors interesting ambipolar materials for application in field effect transistors and photovoltaic cells.

Ambipolarity in low and high molecular mass semiconductors is still a relatively rare feature that is sought after for many applications in organic electronics. From this point of view, compounds containing arylene bisimide and

[a] Dr. R. Rybakiewicz
Cardinal Stefan Wyszynski University
Faculty of Mathematics and Natural Sciences. School of Exact Sciences
Woycickiego 1/3, 01-938 Warsaw (Poland)
E-mail: r.rybakiewicz@uksw.edu.pl
[b] Dr. R. Rybakiewicz, L. Skorka, Prof. A. Pron, Prof. M. Zagorska,
Faculty of Chemistry, Warsaw University of Technology
Noakowskiego 3, 00-664 Warsaw (Poland)
E-mail: apron@ch.pw.edu.pl
[c] Dr. E. D. Glowacki
Department of Science and Technology, Campus Norrköping,
Linköpings Universitet, Bredgatan 33, SE-601 74 Norrköping, (Sweden)
E-mail: eric.glowacki@liu.se
[d] S. Pluczyk, P. Zassowski, Prof. M. Lapkowski
Silesian University of Technology
Faculty of Chemistry, Strzody 9, 44-100 Gliwice (Poland)
[e] D. H. Apaydin
Linz Institute for Organic Solar Cells (LIOS), Physical Chemistry
Johannes Kepler Universität
Altenbergerstrasse 69, Linz (Austria)
[f] Prof. M. Lapkowski
Centre of Polymer and Carbon Materials, Polish Academy of Sciences
M. Curie-Sklodowska 34, 41-819 Zabrze (Poland)

dithienopyrrole moieties are very interesting. In this paper we report on new DA derivatives, namely naphthalene symmetrically disubstituted with dithienopyrrole and unsymmetric naphthalene derivative functionalized with dithienopyrrole on one side and aliphatic amine on the other side. The former can be considered as a DAD analogue of the ADA compound described by Polander et al.[17] We also present its electrochemical oxidative polymerization. A similar alternating polymer, containing however twice shorter donor unit, was synthesized through Stille coupling of stannylated derivative of dithienopyrrole and dibromoderivative of naphthalene bisimide.[18] In addition to the description of synthetic procedures, we present detailed electrochemical and spectroelectrochemical data obtained for these new low and high molecular weight compounds.

Results and Discussion

Synthesis

Both derivatives 2,6-bis{2-(*N*-(2-ethylhexyl)dithieno[3,2-*b*:2',3'-*d*]pyrrole}-*N,N'*-bis(2-ethylhexyl)-1,4,5,8-naphthalene-tetracarboxylic acid bisimide (**NBI-(DTP)$_2$**) and 2-(2-ethylhexylamino)-6-{2-(*N*-(2-ethylhexyl)dithieno[3,2-*b*:2',3'-*d*]pyrrole}-*N,N'*-bis(2-ethylhexyl)-1,4:5,8-naphthalene-tetracarboxylic acid bisimide (**NBI-DTP-NHEtHex**) were prepared by Stille coupling of the corresponding building blocks *i.e.* 2-(tributylstannyl)-*N*-(2-ethylhexyl)-dithieno[3,2-*b*:2',3'-*d*]pyrrole (**3**) with *N,N'*-bis(2-ethylhexyl)-2,6-dibromo-1,4,5,8-naphthalenetetracarboxylic acid bisimide (**5**) or *N,N'*-bis(2-ethylhexyl)-2-bromo-6-(2-ethylhexylamino)-1,4,5,8-naphthalenetetracarboxylic acid bisimide (**6**) in the cases of **NBI-(DTP)$_2$** and **NBI-DTP-NHEtHex**, respectively. The synthetic routes are depicted in Scheme 1.

Compounds **1** - **5** were prepared according to published procedures or their slight modifications (see experimental part for details). For **6** a special, one-step procedure was elaborated enabling its preparation in the reaction between naphthalene dianhydride (**4**) and 2-ethylhexylamine with 42% yield.

Optical properties - experiment *vs* DFT calculations

UV-vis spectra of naphthalene bisimides with no substituents in the core are characterized by a strong absorption band of a vibronic character, ascribed to the arylene $\pi-\pi^*$ transition, with the *0-0* vibronic peak, in the vicinity of 380 nm, showing the highest intensity.[19] Core functionalization of these compounds with electron-donating substituents gives rise to a new band at significantly longer wavelengths, usually of charge transfer (CT) character.[6b,20] This CT band with a maximum at 689 nm is also clearly seen in the spectrum of **NBI-(DTP)$_2$** (Figure 1a). Two other features of this spectrum should be noticed: i) the $\pi-\pi^*$ band of the naphthalene bisimide core is slightly bathochromically shifted to 389 nm for the *0-0* transition and the *0-1* transition band at 371 nm becomes dominant, broadening of these peaks is observed which makes the vibronic structure less pronounced; ii) a rather broad band at 305 nm is unequivocally ascribed to the presence of dithienopyrrole substituents, based on the comparison with the spectrum of *N*-(2-ethylhexyl)dithieno[3,2-*b*:2',3'-*d*]pyrrole **(2)** (Figure 1a). In the spectrum of **NBI-DTP-NHEtHex** all peaks *i.e.* the CT band, the core $\pi-\pi^*$ band and the substituent bands are hipsochromically shifted with respect to the analogues bands in the spectrum of **NBI-(DTP)$_2$** (compare Figures 1a and b). This is consistent with the lower optical band gap of the former.

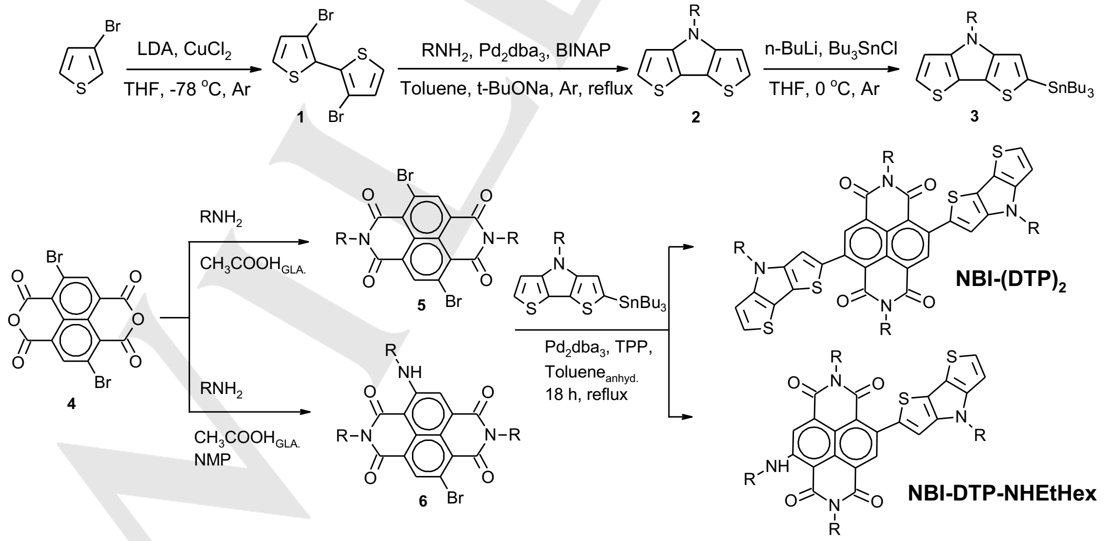

Scheme 1. Synthetic routes to **NBI-(DTP)$_2$** and **NBI-DTP-NHEtHex** (R = C_8H_{17}).

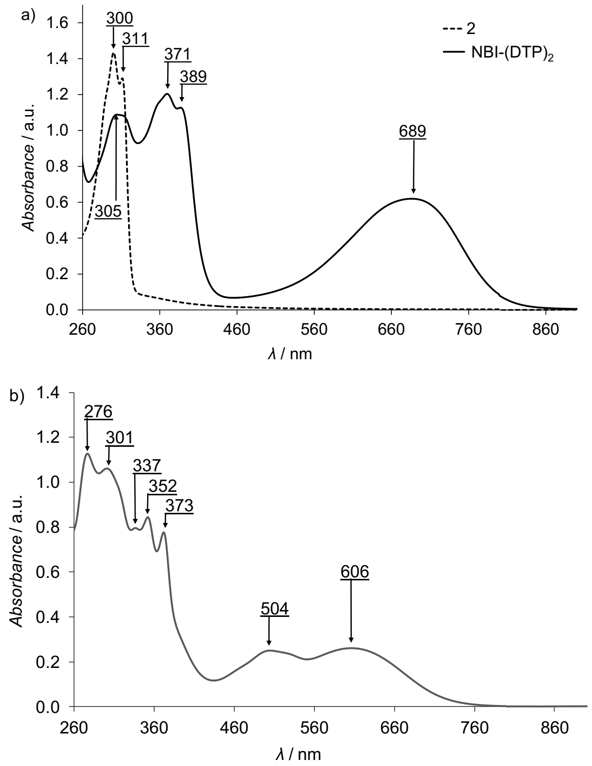

Figure 1. UV-vis spectrum of: (a) **NBI-(DTP)$_2$** and N-(2-ethylhexyl)dithieno[3,2-b:2',3'-d]pyrrole (**2**); (b) **NBI-DTP-NHEtHex** in $CHCl_3$.

A comparison of the experimental findings with the results of quantum calculations using B3LYP/6-31G(d) indicates a fair agreement between the experiment and the theory for the bands of higher energy. However, the theoretically predicted CT bands energies are underestimated for both studied compounds (see Figure S1 and S2). The use of an alternative set of calculations (CAM-B3LYP/6-31G(d)), frequently employed to the calculation of theoretical spectra in DA-type conjugated molecules[6,21,22] does not improve the agreement between the experiment and the theory. The calculations accurately predict, however, the oscillator strength, *f*, of the CT band. In the case of **NBI-(DTP)$_2$** *f* is more than twice higher than for **NBI-DTP-NHEtHex**, following the experimental trend (see Table S1 and S2 in Supporting Information). This difference is partially caused by higher symmetry of **NBI-(DTP)$_2$**. The charge transfer in this molecule is a $A_u \rightarrow A_g$ transition, which is strongly favored due to the Laporte selection rule. In the case of **NBI-DTP-NHEtHex**, the dual nature of the CT band can be explained as a superposition of transfer from DTP to NBI (the less energetic one) and from NH to NBI (the more energetic one). DFT calculations additionally indicate that the CT transitions are purely (**NBI-(DTP)$_2$**) or almost purely (99% in **NBI-DTP-NHEtHex**) HOMO→LUMO in nature. A comprehensive list of the most significant vertical excitations along with NTO analysis is presented in Supporting Information (Table S1 and S2).

Cyclic voltammetry and EPR spectroelectrochemistry *vs* DFT calculations

Cyclic voltammetric measurements were performed in 10^{-3} M solution of the studied compounds in 0.1 M Bu_4NBF_4/CH_2Cl_2 electrolyte using platinum working and counter electrodes and Ag/Ag^+ as a reference electrode. Figure 2a shows a representative, solution voltammogram of **NBI-(DTP)$_2$**, registered at negative potentials (*vs* Fc/Fc^+). Two consecutive and reversible redox couples can be observed at negative potentials with formal redox potentials equal to E^0_1 = -1.06 V and E^0_2 = -1.46 V *vs* Fc/Fc^+ with spacing between the reduction and the corresponding oxidation peak equal to *ca.* 0.60 V. They can be ascribed to two consecutive one-electron transfers to the bisimide core, leading to the formation of a radical anion in the first step and a spinless dianion in the second one.[23] In arylene bisimides the distance between the first and the second reduction peaks is strongly dependent on the size of bisimide core, since it determines the capability of delocalizing of the surplus electron density imposed on the molecule during its reduction to a radical anion and facilitates the addition of the second electron to form a dianion.[23] In the case of **NBI-(DTP)$_2$** the value of $E_{red1} - E_{red2}$ is by 0.05 to 0.08 V lower than in naphthalene bisimides that are not core-functionalized.[19,22] This may suggest that the radical anion charge density is partially delocalized from the core to dithienopyrrole substituents, as corroborated by the DFT calculations of unpaired spin density distribution (*vide infra*). The electrochemical data, concerning the negative potential range, are collected in Table 1. In the positive potential range (Figure 2b), **NBI-(DTP)$_2$** undergoes oxidative polymerization, which is manifested by two overlapping anodic peaks at E = 0.54 V and 0.61 V. In the reverse scan, two cathodic peaks appear at E = 0.48 V and 0.17 V originating from the reduction of the polymeric layer, deposited on the electrode in the oxidated state. The electropolymerisation process will be described in greater detail in the next section of this paper.

In the cyclic voltammogram of **NBI-DTP-NHEtHex** (Figure 3a) two reversible redox couples, corresponding to two consecutive one electron reductions, appear at -1.29 V and -1.69 V, *i.e.* at significantly lower potentials than in the case of **NBI-(DTP)$_2$** (Table 1). This effect clearly reflects stronger electron-donating properties of the aliphatic amine substituent as compared to DTP. At positive potentials one irreversible anodic peak is observed with a maximum at 0.47 V (Figure 3b).

For both molecules studied the formation of radical anions in the first step of the reduction process was confirmed by EPR spectroelectrochemical experiments. Lowering the working electrode potentials to the values close to the maximum of the first reduction peak (-1.1 V and -1.3 V *vs* Fc/Fc^+ for **NBI-(DTP)$_2$** and **NBI-DTP-NHEtHex**, respectively) generates radical anions, whose presence in the solution can be spectroscopically detected. In Figure 4a a representative EPR spectrum of the radical anion form of **NBI-DTP-**

10.1002/chem.201604672

NHEtHex is shown. It closely resembles the spectrum of unsymmetric naphthalene bisimide derivative with the same 2-ethylhexylamine substituent on one side of the core and triphenylamine on the other.[6b] The registered spectrum shows a clear multi-line character which means that no microsegregation of the bisimide molecules occurs during their reduction to radical anions. In addition rapid reorientation of the formed radical anions must occur leading to the removal of anisotropic contributions to the *g*-factor and hyperfine interactions. The observed spectral pattern could be simulated assuming isotropic hyperfine interactions of the unpaired spin with all three nitrogen and four hydrogens. The corresponding coupling constants are shown in Figure S3 in the Supporting Information and collected in Table 2.

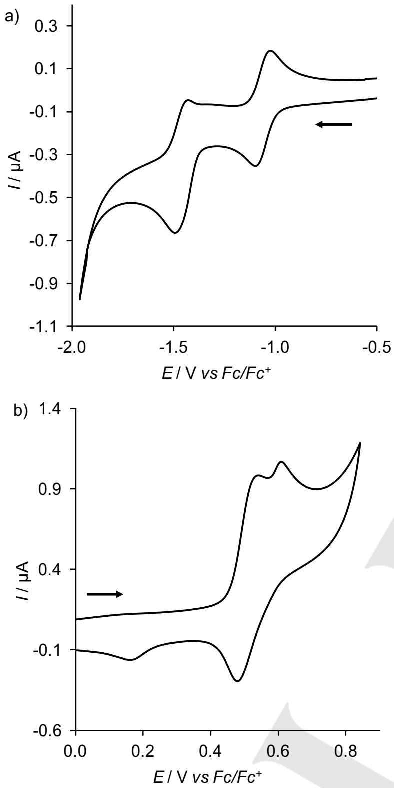

Figure 2. Cyclic voltammograms of 1×10^{-3} M **NBI-(DTP)$_2$** in the negative (a) and positive (b) potential ranges. Scan rate 50 mV/s, electrolyte 0.1 M Bu_4NBF_4 in CH_2Cl_2.

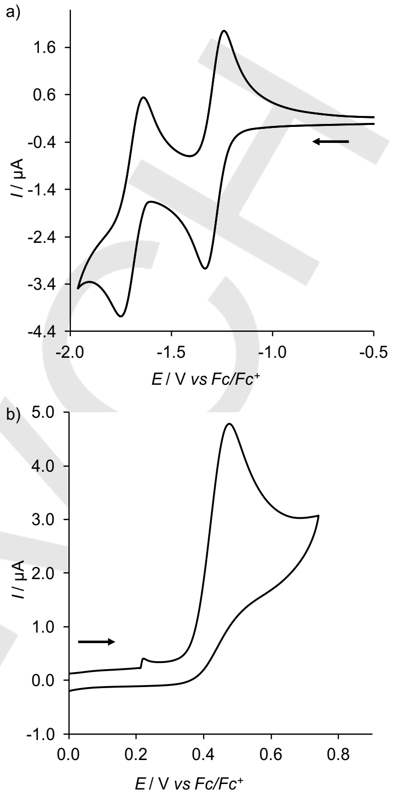

Figure 3. Cyclic voltammograms of 1×10^{-3} M **NBI-DTP-NHEtHex** in the negative (a) and positive (b) potential ranges. Scan rate 50 mV/s, electrolyte 0.1 M Bu_4NBF_4 in CH_2Cl_2.

NBI-(DTP)$_2$, upon its reduction to a radical anion, yields a broad unresolved line which can be treated as a superposition of several signals showing very small hyperfine coupling coefficients (see Figure 4b). It is possible that in the case of the symmetric derivative the unpaired spin interacts with a larger number of hydrogens as compared to the case of **NBI-DTP-NHEtHex**.

Unresolved and rather weak EPR line was registered upon oxidation of **NBI-DTP-NHEtHex** at E = +0.7 V, evidently due to the irreversibility of this process which has to involve consecutive reactions of the formed radical cation (see Figure 4c). No EPR data could be collected for **NBI-(DTP)$_2$** in the oxidative mode, since in this case the electropolymerization process interfered.

Table 1. Cyclic voltammetry data of the studied dithienopyrrole-substituted naphthalene bisimides in the negative potentials range. Potentials given *vs* Fc/Fc$^+$.

Compound	E_{red1} / V	E_{ox1} / V	1/2(E_{red1} + E_{ox1}) / V	E_{red2} / V	E_{ox2} / V	1/2(E_{red2} + E_{ox2}) / V
NBI-(DTP)$_2$	-1.09	-1.03	-1.06	-1.48	-1.43	-1.46
NBI-DTP-NHEtHex	-1.33	-1.24	-1.29	-1.74	-1.64	-1.69

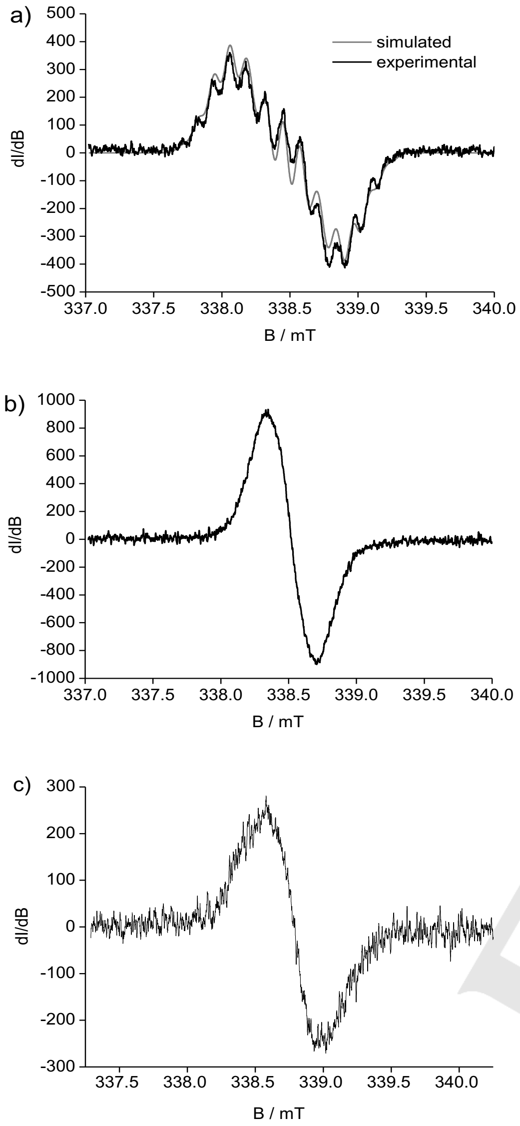

Figure 4. EPR spectra of: (a) radical anion form of **NBI-DTP-NHEtHex**, experimental (black line) and simulated (gray line), E = -1.3 V; (b) radical anion of **NBI-(DTP)$_2$**, E = -1.1 V; (c) radical cation form of **NBI-DTP-NHEtHex**, E = +0.7 V. Concentrations of studied compounds 1×10^{-3} M, electrolyte 0.1M Bu_4NPF_6/CH_2Cl_2, E *vs* Fc/Fc$^+$.

Table 2. EPR parameters of radical anion forms of **NBI-DTP-NHEtHex** and **NBI-(DTP)$_2$** and radical cation form of **NBI-DTP-NHEtHex**.

Radical ion	Hfcc / mT	Linewidth / mT	*g*-factor
NBI-(DTP)$_2$$^{-\cdot}$	–	–	2.0036
NBI-DTP-NHEtHex $^{-\cdot}$	N: 0.108; 0.108; 0.121 H: 0.402; 0.164; 0.101; 0.102	0.052	2.0036
NBI-DTP-NHEtHex $^{+\cdot}$	–	–	2.0027

A comparison of the voltammograms of **NBI-(DTP)$_2$** and **NBI-DTP-NHEtHex** with those recorded for dithienopyrrole and its oligomers[24] and for naphthalene bisimide with electrochemically inactive substituents[19] as well as the EPR spectroelectrochemical results, indicate that the reduction takes place in the bisimide core whereas the oxidation - on the substituent. This implies at least partial spatial separation of the HOMO and LUMO orbitals. We were therefore tempted to verify whether DFT calculations would reflect the electrochemical findings. In these calculations the geometries were optimized both in vacuum and solution of dichloromethane (for comparisons with CV studies) and chloroform (TD-DFT). The structures were generated without any simplification *i.e.* taking into consideration all alkyl chains. As expected, due to sterical reasons, the dithienopyrrole substituents are twisted with respect to the core in order to release repulsions. The dihedral angles are equal to 45.25° and to 47.30° for **NBI-(DTP)$_2$** and **NBI-DTP-NHEtHex**, respectively. Molecular orbitals contours are presented in Figure 5. In both cases spatial separation of frontier orbitals is evident, with HOMO predominantly lying on the dithienopyrrole substituents whereas LUMO predominantly occupying the core NBI fragment.

The localization of the charge generated upon one electron reduction or oxidation can be further traced with the spin-density maps presented in Figure 6. In the radical cation form, the spin density is mainly located on the dithienopyrrole substituents with smaller extension to the two central rings of the core. The radical anion spin density, in turn, predominantly occupies the core, however its extension to the dithienopyrrole substituents is evident. This extended delocalization explains diminishing of the spacing between the first and the second reduction peaks in the cyclic voltammogram of **NBI-(DTP)$_2$**, as already indicated.

Table 3. Comparison of the theoretical and experimental HOMO/LUMO, ionization potential (IP), electron affinity (EA) and energy gaps (E_g) of **NBI-(DTP)$_2$** and **NBI-DTP-NHEtHex**.

		Theoretical data					Experimental data		
Compound	medium	HOMO /eV	LUMO /eV	E_g /eV	IP /eV	EA /eV	IP^a /eV	EA^b /eV	E_g/eV
NBI-(DTP)$_2$	Vacuum	-5.02	-3.09	1.93	5.86	-2.19	–	–	–
	CH_2Cl_2	-5.11	-3.25	1.87	5.02	-3.36	5.09	-3.64	1.52^c 1.45^d
NBI-DTP-NHEtHex	Vacuum	-5.04	-2.94	2.10	6.04	-1.99	–	–	–
	CH_2Cl_2	-5.13	-3.03	2.10	5.02	-3.17	5.01	-3.42	1.65^c 1.59^d

^{a}calculated from the onset of the first oxidation peak, using equation: IP = /q/($E^0_{ox3,\ onset}$ + 4.8) /eV; ^{b} calculated from the onset of the first reduction peak using equation: EA = -/q/($E^0_{red1,\ onset}$ + 4.8) /eV; ^{c}data calculated from absorption band onset; ^{d}data determined from cyclic votammetry.

In Table 3 the theoretical data are compared with the experimental ones, determined from the onset of the first reduction peak (electron affinity - EA) and the first oxidation peak (ionization potential - IP) in the corresponding voltammogram (Figures 2 and 3). The calculations correctly predict larger band gap in **NBI-DTP-NHEtHex** than for **NBI-(DTP)$_2$** and its smaller |EA| value. In general, the observed trends are consistent with the experiment although the theoretical band gaps are slightly overestimated, whereas |EA| - underestimated.

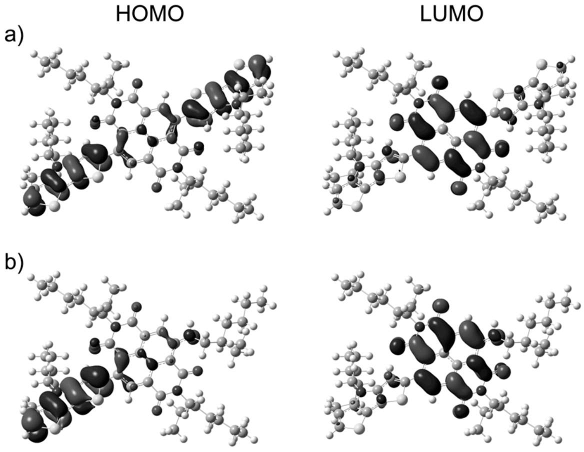

Figure 5. The graphical representation of HOMO and LUMO contours of **NBI-(DTP)$_2$** (a) and **NBI-DTP-NHEtHex** (b) calculated at B3LYP/6-31G(d) level of theory (isosurface value = 0.03, light and dark grey stand for negative and positive wavefunction sign, respectively). Figure S4 in the Supporting Information shows all pictures in color.

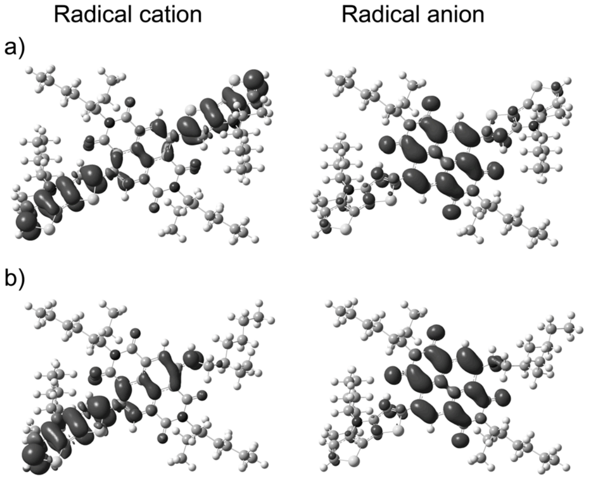

Figure 6. Spin density maps (isovalue = 0.001, dark and light grey stand for negative and positive density, respectively) **for NBI-(DTP)$_2$** (a) and **NBI-DTP-NHEtHex** (b); upon oxidation (left) and reduction (right). Figure S5 in the Supporting Information shows all pictures in color.

Electropolymerization of NBI-(DTP)$_2$ and spectroelectrochemical properties of the resulting product

Upon repeated cycling in the potential range from -1.80 V to 0.70 V (*vs* Fc/Fc$^+$) **NBI-(DTP)$_2$** electropolymerizes with simultaneous deposition of an electrochemically active film on the working electrode. The polymer thickness increases with each cycle. Figure 7 shows first 10 scans of the electrochemical polymerization process.

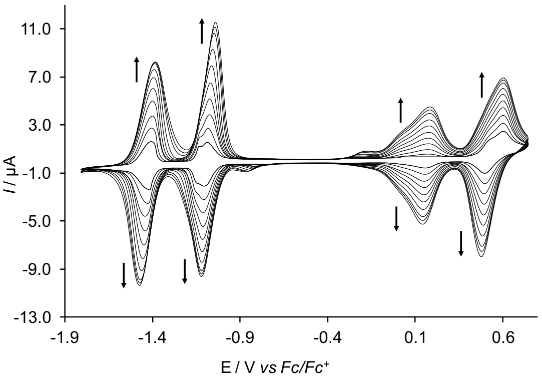

Figure 7. Potentiodynamic electropolymerization of **NBI-(DTP)$_2$** on a platinum electrode immersed in 0.1 M Bu_4NBF_4/CH_2Cl_2 electrolyte containing 1×10^{-3} M of **NBI-(DTP)$_2$**. Scan rate: 50 mV/s.

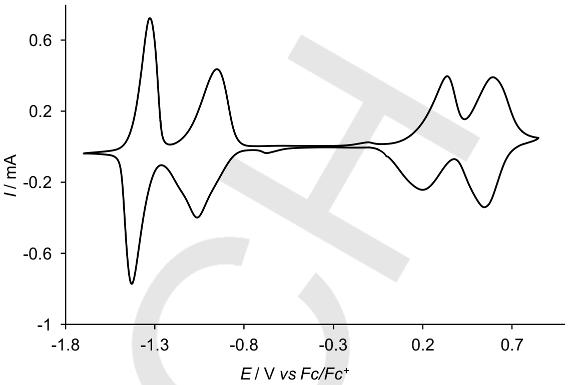

Figure 8. Cyclic voltammogram of a thin film of **poly(NBI-(DTP)$_2$)** deposited on a platinum plate electrode. Electrolyte 0.1 M Bu_4NBF_4/CH_3CN Scan rate 50 mV/s.

Since electropolymerization occurs through the formation of radical cations at the terminal thiophene rings followed by their coupling, the presence of electron-donating pyrrole moiety at the adjacent position facilitates this process by lowering the electropolymerization potential.

A representative cyclic voltammogram of a thin film of **poly(NBI-(DTP)$_2$)**, registered without the presence of the monomer is presented in Figure 8. A very interesting electrochemical behaviour of this polymer should be pointed out. It exhibits two reversible redox couples at +0.27 V and +0.58 V (*vs* Fc/Fc$^+$) in the oxidative regime and equally two reversible couples at -0.99 V and -1.38 V (*vs* Fc/Fc$^+$) (see Table 4) in the reductive one. Moreover, this polymer has electrochromic properties, showing at different potentials several stable colors (see Figure S6).

Taking into account that all four redox couples are reversible in an aprotic solvent (acetonitrile) and show essentially the same area in the cyclic voltammogram, we are tempted to ascribe them to two consecutive one-electron reductions to a radical anion and dianion at negative potentials and to two one electron oxidations to a radical cation and dication at positive ones (see Scheme 2 and 3).

Donor-acceptor interactions, combined with extended conjugation, make **poly(NBI-(DTP)$_2$)** a low band-gap copolymer showing IP of 5.01 eV (determined from the onset of the first oxidation peak), $|EA|$ of 3.90 eV (determined from the onset of the first reduction peak) and the electrochemical band gap equal to 1.11 eV *i.e.* by more than 0.30 eV narrower than the gap of its monomer (**NBI-(DTP)$_2$**) (see Table 3).

Table 4. Cyclic voltammetry data of the redox couples associated with the reduction and oxidation of **poly(NBI-(DTP)$_2$)**. Potentials given *vs* Fc/Fc$^+$.

Compound	E_{red1} / V (0/-1)	E_{ox1} / V (-1/0)	1/2(E_{red1} + E_{ox1}) / V	E_{red2} / V (-1/-2)	E_{ox2} / V (-2/-1)	1/2(E_{red2} + E_{ox2}) / V
poly(NBI-(DTP)$_2$) reduction	-1.04	-0.93	-0.99	-1.40	-1.35	-1.38
Compound	E_{ox3} / V (0/+1)	E_{red3} / V (+1/0)	1/2(E_{ox3} + E_{red3}) / V	E_{ox4} / V (+1/+2)	E_{red4} / V (+2/+1)	1/2(E_{ox4}+ E_{red4}) / V
poly(NBI(DTP)$_2$) oxidation	+0.32	+0.21	+0.27	+0.60	+0.55	+0.58

10.1002/chem.201604672

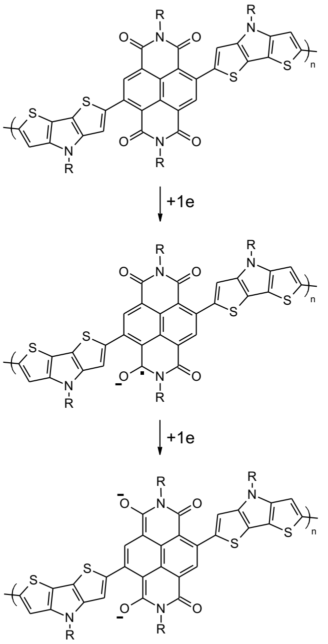

Scheme 2. Two-step, two electron reduction of **poly(NBI-(DTP)$_2$)** with the formation of a radical anion in the first step and a spinless dianion in the second one.

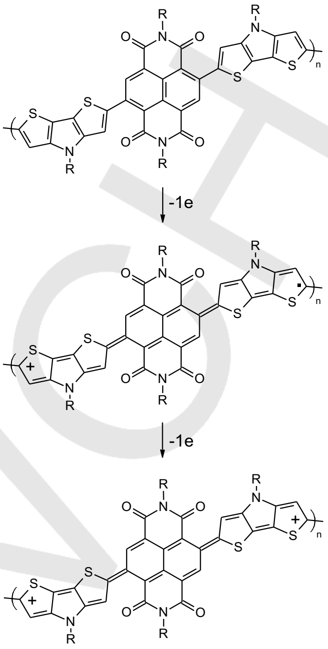

Scheme 3. Two-step, two electron oxidation of **poly(NBI-(DTP)$_2$)** with the formation of a radical cation in the first step and a spinless dication in the second one.

Radical anions generated in the first reduction process are stable enough to be detected in an *in situ* electrochemical - EPR experiment. Figure 9 shows the growth of the EPR line upon scanning the electrode potential in the range corresponding to the first reduction peak in the corresponding cyclic voltammogram. The EPR line appears at the onset potential of the first reduction process and reaches the highest intensity at the potential of the first reduction peak maximum.

Potentiostatic reduction at E = -1.00 V *vs* Fc/Fc$^+$ yields a clear EPR signal which can be fitted assuming three non-equivalent paramagnetic centers of unequal contribution (for details see the Supporting Information Figure S7). This non-equivalence evidently arises from the high molecular mass nature of **poly(NBI-(DTP)$_2$** which imposes differences in local conformations of the macromolecules in the solid state.

Since the second reduction state of **poly(NBI-(DTP)$_2$)** (dianion) is spinless, its investigation by EPR gives no information apart from a decrease of the EPR line intensity to zero caused by gradual transformation of radical anions into dianions. For this reason, complementary UV-vis-NIR spectroelectrochemical studies were carried out with the goal to identify diagnostic spectral features of radical anions and dianions. The spectrum of the polymer neutral form is significantly different from that of the monomer (see spectrum registered at E = -0.45 V *vs* Fc/Fc$^+$ in Figure 10a).

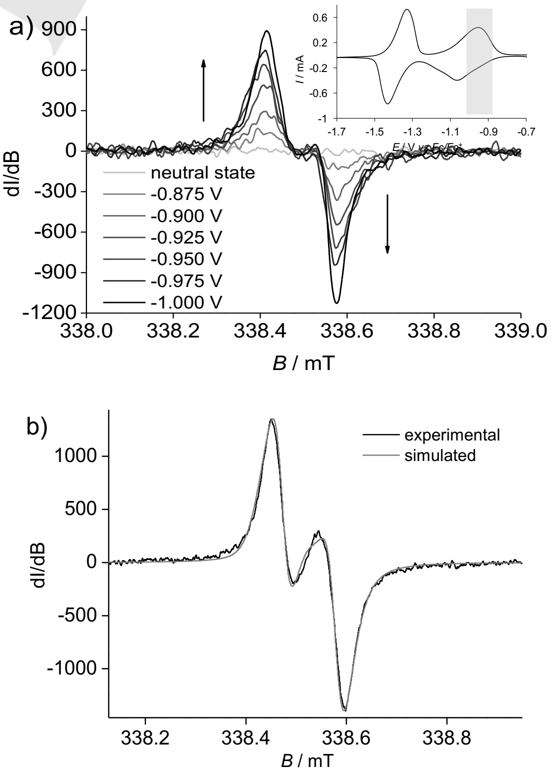

Figure 9. (a) Changes in EPR spectra registered during potentiodynamic reduction of **poly(NBI-(DTP)$_2$)** deposited on a platinum electrode *via* electrochemical polymerization. Electrolyte 0.1 M Bu_4NPF_6/CH_2Cl_2, E *vs* Fc/Fc$^+$; (b) simulation of the EPR signal generated during potentiostatic reduction of this polymer at E = -1.0 V *vs* Fc/Fc$^+$.

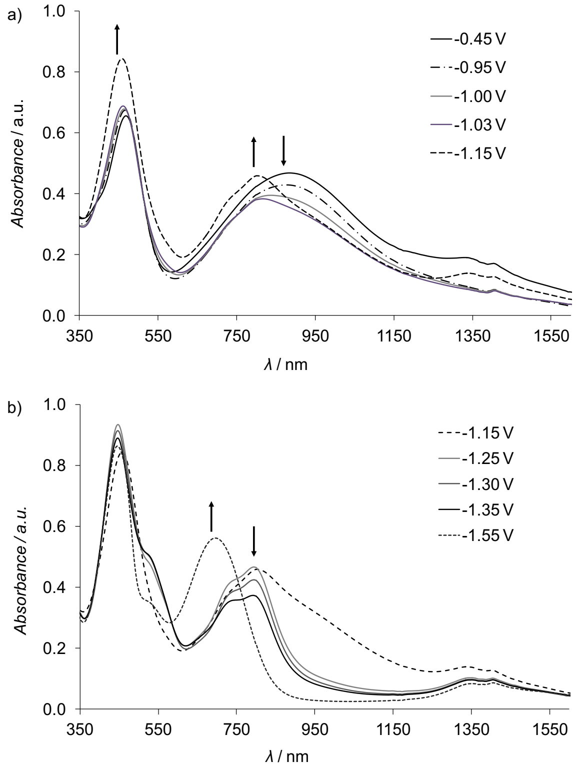

Figure 10. UV-vis-NIR spectra of a thin film of **poly(NBI-(DTP)$_2$)**, deposited on an ITO electrode and registered for decreasing electrode potential: (a) potentials range from -0.45 V to -1.15 V; (b) from -1.15 V to -1.55 V. Electrolyte 0.1 M Bu_4NBF_4/CH_3CN, E *vs* Fc/Fc$^+$.

First, the band characteristic of the dithienopyrrole moiety at 308 nm in the monomer and its characteristic naphthalene core band at 380 nm, showing a clear vibronic structure, merge into one, featureless band which is bathochromically shifted to 468 nm. Similarly, the CT band located at 689 nm in the monomer is shifted to 885 nm in the polymer. All these changes are caused by a significant extension of the conjugation combined with DA interactions. In the polymer chain, which shows -(DDA)- structure, the donor segment doubles its length since it consists of two dithienopyrrole units. Lowering the electrode potential in the range corresponding to the formation of radical anions (Figure 10a) results in a gradual decrease of the CT band and a growth of a band peaked at 803 nm with a broad tail extending towards NIR part of the spectrum. Simultaneously the band at lower wavelengths is being hypsochromically shifted from 468 nm in the neutral polymer to 458 in its poly(radical anion) form. In Figure 10b further evolution of the spectra is presented, when the ITO electrode potentials reach the potentials range of the second reduction step. In this potential range a gradual decrease of the band characteristic of the radical anion state occurs with quick and complete bleaching of its longer wavelength tail. A new band appear: at *ca.* 740 - 750 nm, which is then hypsochromically shifted to 696 nm at the final state of the reduction. The high-energy band is being further hyspochromically shifted to 446 nm with clear appearance of a shoulder at longer wavelengths. Positions of the bands diagnostic of the neutral, radical anion and dianion states of **poly(NBI-(DTP)$_2$)** are listed in Table 5.

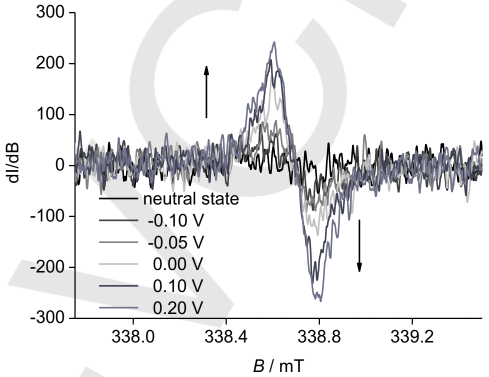

Figure 11. Changes in EPR spectra registered during potentiodynamic oxidation of **poly(NBI-(DTP)$_2$)** deposited on a platinum electrode *via* electrochemical polymerization. Electrolyte 0.1 M Bu_4NPF_6/CH_2Cl_2, E *vs* Fc/Fc$^+$.

Ambipolarity of poly(NBI-(DTP)$_2$) is manifested by the fact that its radical cation state can be electrochemically generated by symmetry to the radical anion one. The EPR signal of the radical cation appears at the potential of the onset of the first oxidation process and increases in intensity up to 0.3 V, i.e. the potential at which the first oxidation process is over, as determined by cyclic voltammetry (see Figure 8). The obtained EPR signals remain unresolved and cannot be deconvoluted.

The formation of radical cations and dications was also followed by UV-vis-NIR spectroelectrochemistry. In Figure 12a spectral changes occurring in the potential range corresponding to the first oxidation step are presented. Electrochemical oxidation of **poly(NBI-(DTP)$_2$)** to the poly(radical cation) state results to a complete bleaching of the band at 468 nm *i.e.* the band originating from π-conjugation. This is consistent with the reduction and oxidation pathway, presented in Schemes 2 and 3. The formation of radical cations and dications completely changes the conjugated bonds sequence, whereas the reduction to radical anions occurs at the periphery of the macromolecule. Their further reduction to dianions only locally influences the π-bonding sequence, leaving the conjugation pathway very little changed. As a result, the π-conjugation band does not disappear during the reduction process but undergoes a small hypsochromic shift (compare Figures 10 and 12). Upon the first oxidation step two new bands appear at 570 nm and *ca.* 1040 nm whereas the CT band undergoes a hypsochromic shift from 885 nm to *ca*. 830 nm. These three bands can be considered as diagnostic of the poly(radical cation) state. In the second oxidation step three bands characteristic of the radical cations diminish in intensity and a new band ascribed to the poly(dication) state appears (see Figure 12b). Positions of the bands diagnostic of radical cations and dications are listed in Table 5.

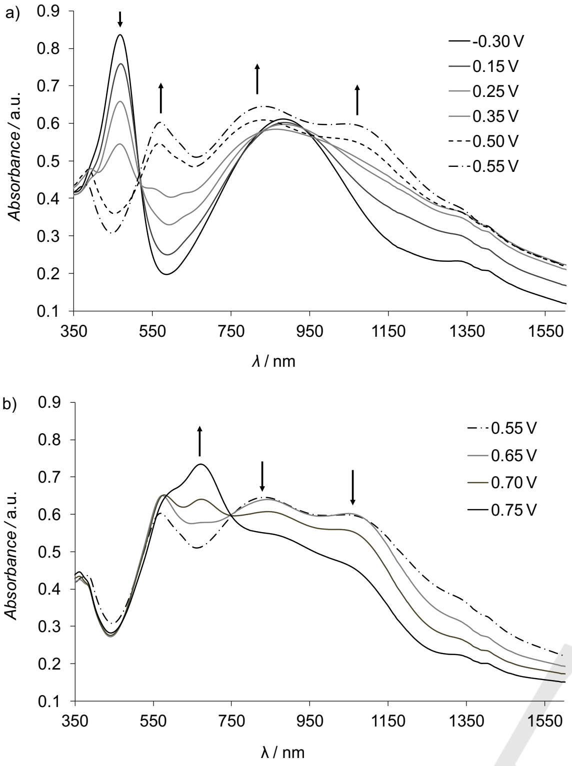

Figure 12. UV-vis-NIR spectra of a thin film of **poly(NBI-(DTP)$_2$)**, deposited on an ITO electrode and registered for increasing electrode potential: (a) potentials range from -0.45 V to +0.55 V; (b) from +0.55 V to +0.75 V. Electrolyte 0.1 M Bu_4NBF_4/CH_3CN, E *vs* Fc/Fc^+.

Table 5. UV-vis-NIR spectroscopic data obtained for **poly(NBI-(DTP)$_2$)** in its neutral, radical anion, dianion radical cation and dication state.

Compound state	λ_{max} / nm of the diagnostic peaks
poly(NBI-(DTP)$_2^{0}$)	468, 885
poly(NBI-(DTP)$_2^{-}$)	458, 803
poly(NBI-(DTP)$_2^{2-}$)	446, 530 (shoulder), 696
poly(NBI-(DTP)$_2^{\cdot+}$)	570, 830, 1040
poly(NBI-(DTP)$_2^{2+}$)	675

To summarize this part of the paper, through electropolymerization of naphthalene bisimide disubstituted with dithienopyrrole we fabricated a low band gap electroactive polymer exhibiting extremely interesting electrochemical behavior manifested by reversible two step - two electron reduction and oxidation, corroborated by complementary EPR and UV-vis-NIR spectroelectrochemical investigations.

Electrochemistry of poly(NBI-(DTP)$_2$) in aqueous electrolytes

For these studies, **poly(NBI-(DTP)$_2$)** was electrochemically deposited on a glass substrate with an evaporated Cr/Au (5nm/80nm) contact. An air-tight cell having a working electrode with the structure of Cr/Au/**poly(NBI-(DTP)$_2$)**, a Pt-plate counter electrode and an Ag/AgCl reference electrode, was assembled and purged with nitrogen for 30 min in all cases. Cyclic voltammograms were recorded in at pH 2, 7, and 10. Electrolyte solutions were prepared using HCl or NaOH, with Na_2SO_4 added to maintain a constant ionic strength of 0.1 M.

Poly(NBI-(DTP)$_2$) bearing electrode was immersed into the electrolyte solution and the cyclic voltammogram was recorded between 0 mV – (-400 mV). Independently of the pH of the medium, the polymer showed a capacitive electrochemical behaviour in water with currents in the range of nA. The reductive electrochemistry of the polymer itself was not reachable since potentials required for reduction of the polymer are more negative than the hydrogen evolution reaction (HER). At pH 2 (Figure 13a), the reductive peak corresponding to HER has an onset of around -300 mV, becoming more negative at pH 7 (Figure 13b), finally at pH 10 the HER onset, as expected, is beyond -400 mV (Figure 13c). Faradaic photocurrents were observed when illuminating with a halogen lamp (~50 mW/cm^2). The effect was always photocathodic, and increases as pH is decreased. Since the experiments were conducted in an oxygen-free electrolyte, we exclude oxygen reduction reactions.[25,26] We therefore attribute the photocathodic effect to HER. Though the photocurrent densities are too small for practical photocatalytic hydrogen evolution, we note that very few reports on conjugated polymers accomplishing HER exist.[27,28] Moreover, the light/dark effects were reversible and no current decrease was observed after several cycles, signaling that this material is relatively stable in aqueous electrolytes.

These preliminary results show that **poly(NBI-(DTP)$_2$)** is stable in a wide range of pH values, even upon repeated cycling in these conditions, showing that such materials may be used to support photocatalysis processes.

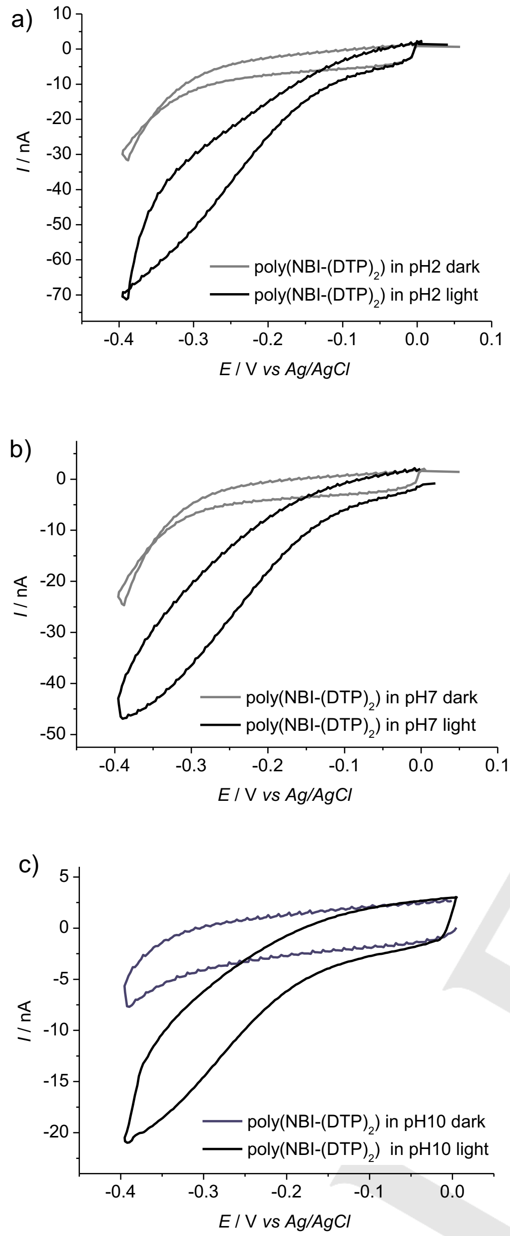

Figure 13. Cyclic voltammograms registered in aqueous electrolytes of different pH without and with illumination: (a) pH = 2; (b) pH = 7; (c) pH = 10.

Diodes fabricated from poly(NBI-(DTP)$_2$)

A thin layer of **poly(NBI-(DTP)$_2$)** was electrochemically deposited on an ITO substrate using 10 potentiondynamic cycles and used for the fabrication of a sandwich-type diode (Figure 14a). Profilometry measurements show that these films are ~150 nm in thickness. Evaporated films of Aluminum or alternatively MoO$_x$/Ag were used as top contacts for the diodes. Dark J-V characteristics (Figure 14b) demonstrated that the polymer has very low conductivity, suggesting that the material is truly intrinsic and lacks residual electrochemical doping. Illumination with a solar simulator with light intensity of 100 mW/cm^2 resulted in a photovoltaic effect and a 10^4-fold increase in conductivity. This increase, combined with the low dark current, suggest applications of the synthesized polymer in photoconductive detectors. Diodes with aluminum top contacts have a light/dark ratio of up to 10^5 in reverse bias (-0.5V). Diodes with MoO$_x$/Ag, though having higher dark current, were found to operate stably in air, with minimal degradation over several weeks of repeated measurements, indicating that **poly(NBI-(DTP)$_2$)** is a reasonably air-stable semiconductor.

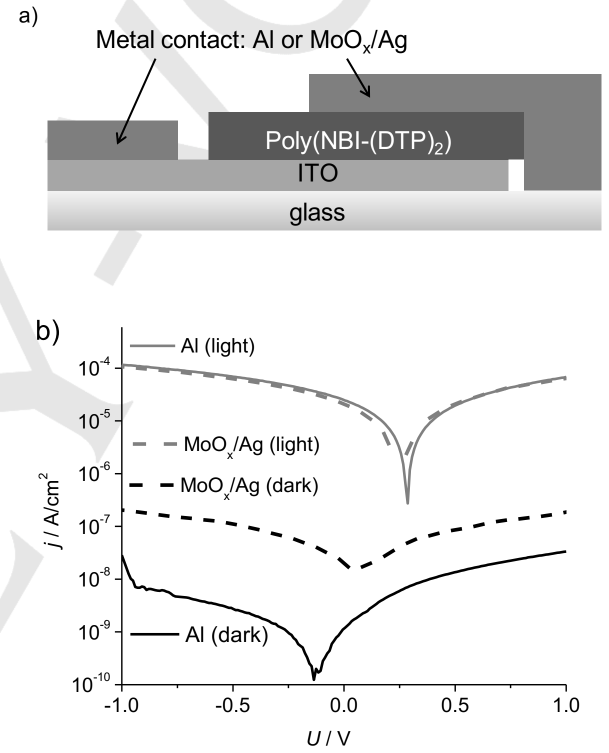

Figure 14. (a) Schematic of sandwich diodes with electrochemically deposited **poly(NBI-(DTP)$_2$)** and sandwiched between ITO and an evaporated top contact. (b) J-V characteristics of diodes with structure as shown in (a) comparing dark J-V curves with illumination by simulated solar illumination, with 100 mW/cm^2.

Conclusions

To summarize, we have synthesized two low molecular weight donor-acceptor electroactive compounds, namely naphthalene bisimide symmetrically core-functionalized with dithienopyrrole (**NBI-(DTP)$_2$**) and an asymmetric core-functionalized naphthalene bisimide with dithienopyrrole substituent on one side and 2-ethylhexylamine on the other side (**NBI-DTP-NHEtHex**). Both compounds showed ambipolarity in their electrochemical behavior due to low band gaps (Eg $_{opt.}$ = 1.52 eV and 1.65 eV, respectively.; Eg $_{electr.}$ =

1.45 eV and 1.59 eV, respectively). **NBI-(DTP)$_2$** could be potentiodynamically electropolymerized to yield an alternating donor-acceptor copolymer **poly(NBI-(DTP)$_2$)** of very low band gap ($E_{g\ electr.}$ = 1.11 eV) and the corresponding IP and $|EA|$ values of 5.01 eV, 3.90 eV, respectively. In cyclic voltammetry this polymers yields four reversible redox couples corresponding to its reduction to poly(radical anion) and poly(dianion) states and to its oxidation to poly(radical cation) and poly(dication) state. The polymer turned out to be electrochemically active also in aqueous solution, showing a distinct photocatalytic current, which did not diminish upon repeated cycling. In diode configuration, the polymer appears stable and truly intrinsic, *i.e.* lacking residual doping, and has a pronounced photoconductivity response. These results taken together show a promising type of DA polymer rich in various electroactive functionality.

Experimental Section

Synthesis

Reagents and chemicals Tris(dibenzylideneacetone)dipalladium(0), 2,2-bis(diphenylphosphino)-1,1-binaphthyl (BINAP), naphthalene 1,4,5,8-tetracarboxylic acid dianhydride, n-butyllithium (2.5 M in hexane), N-methylpyrrolidone (NMP), bromine, tributyltin chloride 96%, lithium diisopropylamide 97%, iodine, triphenylphosphine, dry tetrahydrofuran were purchased from Aldrich. Anhydrous copper chloride (II) was acquired from Chempur. Sodium t-butoxide was obtained from Merck. Glacial acetic acid and toluene were received from POCH. Preparative column chromatography was performed on a glass column with Merck silica gel, 230 – 400 mesh.

3,3'-dibromo-2,2'-bithiophene (**1**), *N*-(2-ethylhexyl)dithieno[3,2-*b*:2',3'-*d*]pyrrole (**2**) and 2-(tributylstannyl)-*N*-(2-ethylhexyl)dithieno[3,2-*b*:2',3'-*d*]pyrrole (**3**) were prepared according to previously reported procedures.[15,24,29] 2,6-dibromo-1,4,5,8-naphthalenetetracarboxylic acid dianhydride (**4**) was obtained by the modified procedures described in the literature.[30] *N,N*'-bis(2-ethylhexyl)-2,6-dibromo-1,4,5,8-naphthalenetetracarboxylic acid bisimide (**5**) was prepared similarly as reported previously.[31] The product was purified by column chromatography (silica gel; CH_2Cl_2/hexane, 8:2, v/v) and obtained as yellow-orange solid (51 % reaction yield).

Synthesis of 2-(tributylstannyl)-N-(2-ethylhexyl)-dithieno[3,2-b:2',3'-d]pyrrole (3) In the three neck flask *N*-(2-ethylhexyl)dithieno[3,2-*b*:2',3'-*d*]pyrrole (2) (0.42 g, 1.72 mmol) was dissolved in dry THF (30 mL). n-BuLi (1.1 ml, 2.75 mmol, 2.5 M in hexane) was added dropwise over 20 minutes at -78 °C in inert atmosphere of argon. Reaction was stirred for 2 hours at room temperature before tributyltin chloride (1.06 g, 2.8 mmol) was added. The mixture was stirred overnight at room temperature. The solution was purified by short column chromatography (silica gel; eluent: hexane + 1 vol% triethylamine) to yield 0.42 g (63%) of light yellow oil.

^{1}H NMR ($CDCl_3$, 400 MHz, ppm): 7.08 (d, 1H); 6.96 (d, 1H); 6.95 (s, 1H); 4.03 - 4.08 (m, 2H); 1.92 – 1.98 (m, 1H); 1.53 - 1.68 (m, 10H); 1.26 - 1.40 (m, 16H); 0.84 - 0.96 (m, 15H).

Synthesis of 2-bromo-6-(2-ethylhexylamino)-N,N'-bis(2-ethylhexyl)-1,4,5,8-naphthalenetetracarboxylic acid bisimide (6) 2,6-dibromo-1,4,5,8-naphthalenetetracarboxylic acid dianhydride (1.2 g, 2.81 mmol) suspended in 20 ml of *N*-methylpyrrolidone was mixed with 20 ml of glacial acetic acid. It was then heated at 60 °C for 20 min and 2-ethylhexylamine (0.91 ml, 7.05 mmol) was consecutively added. The temperature was raised to 120°C and the reaction was carried out for additional 12 h with constant stirring and under argon atmosphere. The reaction mixture was then poured into 200 ml of water and the precipitated product was filtered. Next, it was washed with methanol and purified using a chromatographic column (silica gel, eluent: methylene chloride/hexane, 4/1) to give the desired product (42 % reaction yield).

^{1}H NMR ($CDCl_3$, 400 MHz, ppm) δ: 10.18 (t, J = 7.6Hz, 1H); 8.85 (s, 1H); 8.28 (s, 1H); 4.18 - 4.06 (m, 4H); 3.49 (t, J = 5.8Hz, 2H); 1.99 - 1.87 (m, 2H); 1.83 - 1.73 (m, 1 H), 1.51 - 1.43 (m, 2H), 1.42 - 1.23 (m, 22H); 1.12 - 0.85 (m, 18H).

Synthesis of 2,6-bis{2-(N-(2-ethylhexyl)dithieno[3,2-b:2',3'-d]pyrrole}-N,N'-bis(2-ethylhexyl)-1,4,5,8-naphthalene-tetracarboxylic acid bisimide (NBI-(DTP)$_2$) In the three neck round botom flask 0.3 g, (0.47 mmol) of *N,N'*-bis(2-etylhexyl)-2,6-dibromo-naphtalene bisimide (4) and 0.66 g (1.41 mmol) of 2-(tributylstannyl)-*N*-(2-ethylhexyl)-dithieno[3,2-*b*:2',3'-*d*]pyrrole (3) were dissolved in toluene (30 mL). The reaction mixture was purged with argon 20 minutes before adding triphenylphosphine (0.07 g, 0.26 mmol) and tris(dibenzylideneacetone)dipalladium(0) (0.034 g, 0.037 mmol). The mixture was stirred at 110 °C for 18 hours under argon atmosphere. After cooling to room temperature the mixture was poured into 50 mL of water and extracted with chloroform (200 mL). Solvent was evaporated in vacuum. The crude product was purified using a chromatographic column (silica gel, and the following eluent: methylene chloride/hexane 1/8 + 1 vol% triethylamine), yielding 50 % of blue solid.

^{1}H NMR ($CDCl_3$, 400 MHz, ppm): 8.84 (s, 1H); 7.35 (s, 1H); 7.22 (d, J = 5.2 Hz, 2H); 6.98 (d, J = 5.2 Hz, 2H); 4.12 - 4.02 (m, 8H); 1.97 -1.94 (m, 4H); 1.44 - 1.42 (m, 32H); 0.95 - 0.87 (m, 24H). ^{13}C NMR ($CDCl_3$, 100 MHz, ppm): 162.8; 162.6; 146.2; 145.1; 140.5; 137.6; 136.8; 127.4; 124.8; 121.9; 118.2; 114.9; 113.2; 110.9; 51.4; 44.6; 40.4; 37.8; 30.7; 28.7; 24.0; 23.1; 14.1, 10.7. IR (cm^{-1}): 3349, 3099, 2858, 2925, 2955, 1435, 1527, 1574, 1380, 1412, 1306, 1199, 1216, 1260, 793, 765, 714. HRMS [ESI$^+$]: Calcd. for $C_{62}H_{76}N_4O_4S_4$; $[M+Na]^+$ 1068.4749, found: 1068.4742. UV-vis ($CHCl_3$): λ_{max}= 304 nm, 369 nm, 387 nm, 686 nm.

Synthesis of 2-(2-ethylhexylamino)-6-{2-(N-(2-ethylhexyl)dithieno[3,2-b:2',3'-d]pyrrole}-N,N'-bis(2-ethylhexyl)-1,4,5,8-naphthalenetetracarboxylic acid bisimide (NBI-DTP-NHEtHex) In the three neck round botom flask 0.08 g, (0.098 mmol) of *N,N'*-2-bis(ethylhexyl)-2-bromo-6-(2-ethylhexylamino)-1,4,5,8-naphtalenetetracarboxylic acid bisimide (**6**) and 0.046 g (0.098 mmol) of 2-(tributylstannyl)-*N*-(2-ethylhexyl)-dithieno[3,2-*b*:2',3'-*d*]pyrrole (**3**) were dissolved in toluene (30 mL). The reaction mixture was purged with argon 20 minutes before adding triphenylphosphine (0.069 g, 0.26 mmol) and tris(dibenzylideneacetone)dipalladium(0) (0.034 g, 0.37 mmol). The mixture was stirred at 110 °C for 18 hours under argon atmosphere. After cooling to room temperature the mixture was poured into 50 ml of water and extracted with chloroform (200 mL). Solvent was evaporated in vacuum. The crude product was purified using a chromatographic column (silica gel, and the following eluent: methylene chloride/hexane 4/1 + 1 vol% triethylamine), yielding 54 % of violet solid.

^{1}H NMR ($CDCl_3$, 400 MHz, ppm): 8.74 (s, 1H); 8.30 (s, 1H); 7.15 (d, J = 4.0 Hz, 2H); 7.12 (s, 1H); 6.99 (d, J = 8.0 Hz, 2H); 4.15-4.05 (m, 6H); 3.52 (t, J = 6.0 Hz 2H); 1.97-1.94 (m, 4H); 1.36-1.28 (m, 34H); 0.93-0.88 (m, 24H). IR (cm^{-1}): 2875, 2930, 2960, 1462, 1486, 1588, 1382, 1283, 1094, 1049, 884, 738, 714. HRMS [ESI$^+$]: Calcd. for $C_{54}H_{74}N_4O_4S_2$; $[M+Na]^+$ 929.5049, found: 929.5033. UV-vis ($CHCl_3$): λ_{max} = 276 nm, 301 nm, 337 nm, 352 nm, 373 nm, 504 nm, 606 nm.

Characterization techniques

400 Hz ^{1}HNMR and ^{13}CNMR spectra were recorded in deuterated chloroform ($CDCl_3$) on Varian Mercury Instrument. FT-IR spectra were recorded on a Perkin-Elmer Paragon 1000 spectrometer equipped with MIRacle ATR sampling accessory. HRMS spectra were recorded in methanol on Mariner ESI-TOF (Applied Biosystems) mass spectrometer using polyethylene glycol 400 (PEG 400) sodiated ions as internal standard. Solution spectra of the obtained compounds, dissolved in chloroform, as well as the solid state spectra of the polymer thin films deposited on an ITO electrode, were recorded on a Varian Cary 5000.

Cyclic voltammetry studies were carried out for the solutions and for thin solid films of all obtained compounds. 1×10^{-3} M solution of **NBI-(DTP)$_2$** or **NBI-DTP-NHEtHex** in 0.1 M Bu_4NBF_4/CH_2Cl_2 electrolyte was placed in a one-compartment, three electrode electrochemical cell with a platinum disk working electrode of the surface area of 3 mm^2, a platinum counter electrode and an Ag/0.1 M Ag^+/acetonitrile reference electrode, whose potential was verified using the ferrocene couple at the end of each set of experiment. Thin films were deposited on a platinum disk or plate electrode by electropolymerization. The measurements were performed using an Autolab potentiostat (Eco Chemie). All operations were carried out under dry argon atmosphere in 0.1 M Bu_4NBF_4/CH_3CN electrolyte.

In the UV-vis-NIR spectroelectrochemical measurements the same counter (Pt) and reference (Ag/0.1 M Ag^+) electrodes, and the same electrolyte (0.1 M Bu_4NBF_4/ CH_3CN) as in the case of cyclic voltammetry studies were used.

EPR measurements were performed in a cylindrical cell equipped with set of electrode: a platinum wire as a working electrode, a platinum spiral as a counter electrode and a silver wire calibrated versus ferrocene/ferrocinium redox couple as a pseudoreference electrode. The EPR spectra of cation and anion radical were recorded during potentiostatic oxidation and reduction respectively. The polymeric films obtained by electrochemical polymerization was also investigated by EPR measurements. Changes in the spectra were observed in potentiodynamic mode. EPR measurements were carried out using JEOL JES-FA 200, X-band CW-EPR spectrometer operating at 100 kHz field modulation. Spectroelectrochemical investigations were made by connected spectrometers described above with Eco Chemie AUTOLAB potentiostat-galvanostat model PGSTAT100N.

DFT calculations were carried out using Gaussian09 Revision D.01[32] package and employing hybrid B3LYP[33] exchange correlation potential combined with 6-31G(d) basis set. Ground-state geometries were fully optimized until a stable local minimum was found, which was confirmed by normal-mode analysis (no imaginary frequencies were present). Symmetry constrains were put wherever possible imposing centrosymetric C_i point group. The ground-state geometries were then optimized in solution using polarizable continuum model (PCM)[34] at the same level of theory with dichloromethane and chloroform as solvents. The oscillator strengths and energies of the vertical singlet excitations were calculated employing time-dependent version (TD) of DFT[35] and again at the same level of theory (B3LYP/6-31G(d)) with chloroform as the solvent. The TD-DFT results were retrieved from output files using GaussSum 2.2.[36] The nature of the multiconfiturational transitions was analyzed with natural transition orbitals.[37] Molecular orbital and spin density plots were generated with GaussView5.0.[38]

Acknowledgement

This work was supported by Polish-Norwegian Research Programme, under grant agreement Pol-Nor/210704/43/2013. MZ and AP acknowledge the financial support of National Centre of Science in Poland (NCN, Grant No. 2015/17/B/ST5/00179). S. Pluczyk is scholar supported by the “Doktoris–scholarship program for an innovative Silesia”, co-financed by European Union within European Social Fund. The Gaussian09 calculations were carried out in the Wroclaw Centre for Networking and Supercomputing, WCSS, Wroclaw Poland. http://www.wcss.wroc.pl, under calculational Grant No. 283. Support from the Austrian FWF within the project TRP 294-N19 and The Knut and Alice Wallenberg foundation – Centre for Molecular Medicine, is gratefully acknowledged.

Keywords: dithienopyrrole, naphthalene bisimide, electropolymerization, aqueous electrochemistry, photodiode

[1] a) C. W. Tang, S. A. VanSlyke, *Appl. Phys. Lett.* **1987**, 51, 913-915; b) J. H. Burroughes, D. D. C. Bradley, A. R. Brown, R. N. Marks, K. Mackay, R. H. Friend, P. I. Burn, A. B. Holmes, *Nature* **1990**, 347, 539-541.

[2] G. Horowitz, D. Fichou, X. Z. Peng, Z. G.Xu, F. Garnier, *Solid State Commun.* **1989**, 72, 381-384; b) F. Garnier, G. Horowitz, X. H. Peng D. Fichou, *Adv. Mater.* **1990**, 2, 592-594.

[3] N. S. Sariciftci, L. Smilowitz, A. J. Heeger, F. Wudl, *Science* **1992**, 258, 1474-1476.

[4] a) L. Dou, Y. Liu, Z. Hong, G. Li, Y. Yang, *Chem. Rev.* **2015**, 115, 12633-12665; b) S. Günes, H. Neugebauer, N. S. Sariciftci, *Chem. Rev.* **2007**, 107, 1324-1338; c) Y.-J. Cheng, S.-H. Yang, Ch.-S. Hsu, *Chem. Rev.* **2009**, 109, 5868-5923; d) P. Bujak, I. Kulszewicz-Bajer, M. Zagorska, V. Maurel, I. Wielgus, Adam Pron, *Chem. Soc. Rev.* **2013**, 42, 8895-8999.

[5] X. Zhan, A. Facchetti, S. Barlow, T. J. Marks, M. A. Ratner, M. R. Wasielewski, S. R. Marder, *Adv. Mater.* **2011**, 23, 268-284

[6] a) A. Pron, R. R. Reghu, R. Rybakiewicz, H. Cybulski, D. Djurado, J. V. Grazulevicius, M. Zagorska, I. Kulszewicz - Bajer, J.-M. Verilhac, *J. Phys. Chem. C* **2011**, 115, 15008-15017; b) S. Pluczyk, P. Zassowski, R. Rybakiewicz, R. Wielgosz, M. Zagorska, M. Lapkowski, A. Pron, *RSC Adv.* **2015**, 5, 7401-7412.

[7] a) S. Pluczyk, W. Kuznik, M. Lapkowski, R. R. Reghu, J. V. Grazulevicius *Electrochim. Acta* **2014**, 135, 487-494; b) V. Cherpak, P. Stakhira, D. Volynyuk, L. Politanskiy, N. Kus, R. R. Reghu, J. V. Grazulevicius, *Opt. Mater.* **2014**, 36, 1511-1514.

[8] W. Yue, W. Jiang, M. Böckmann, N. L. Doltsinis, Z. Wang, *Chem. Eur. J.* **2014**, 20, 5209-5213.

[9] H. Dinçalp, Z. Aşkar, C. Zafer, S. İçli, *Dyes and Pigments* **2011**, 91, 182-191.

[10] a) J. Shao, G. Wang, K. Wang, C. Yang, M. Wang, *Polym. Chem.* **2015**, 6, 6836-6844; b) K. Nakabayashi, M. Yamada, H. Mori, *Bull. Chem. Soc. Jpn* **2015**, 88, 222-226.

[11] E. Sefer, F. B. Koyuncu, *Electrochim. Acta* **2014**, 143, 106-113.

[12] Z. Chen, Y. Zheng, H. Yan, A. Facchetti, *J. Am. Chem. Soc.* **2009**, 131, 8-9.

[13] a) Y. Li, W. Xu, S. D. Motta, F. Negri, D. Zhu, Z. Wang, *Chem. Comm.* **2012**, 48, 8204-8206; b) H. Choi, S. Paek, J. Song, C. Kim, N. Cho, J. Ko, *Chem. Commun.* **2011**, 47, 5509-5511.

[14] a) X. Guo, M. D. Watson, *Org. Lett.* **2008**, 10, 5333-5336; b) Y. Wei, Q. Zhang, Y. Jiang, J. Yu, *Macromol. Chem. Phys.* **2009**, 210, 769 - 775; c) X. Zhan, Z. Tan, B. Domercq, Z. An, X. Zhang, S. Barlow, Y. Li, D. Zhu, B. Kippelen, S. R. Marder, *J. Am. Chem. Soc.* **2007**, 129, 7246-7247.

[15] S. C. Rasmussen, S. J. Evenson, *Prog. Polym. Sci.* **2013**, 38, 1773-1804.

[16] X. Zhan, Z. Tan, E. Zhou, Y. Li, R. Misra, A. Grant, B. Domercq, X.-H. Zhang, Z. An, X. Zhang, S. Barlow, B. Kippelen, S. R. Marder, *J. Mater. Chem.* **2009**, 19, 5794-5803.

[17] L. E. Polander, S. P. Tiwari, L. Pandey, B. M. Seifried, Q. Zhang, S. Barlow, C. Risko, J.-L. Brédas, B. Kippelen, S. R. Marder, *Chem. Mater.* **2011**, 23, 3408-3410.

[18] M. Zhou, J. Huang, D. Xu, CN 102344553, **2012**.

[19] P. Gawrys, D. Djurado, J. Rimarčik, A. Kornet, D. Boudinet, J.-M. Verilhac, V. Lukes, I. Wielgus, M. Zagorska, A. Pron, *J. Phys. Chem. B* **2010**, 114, 1803-1809.

[20] C.-C. Lin, M. Velusamy, H.-H. Chou, J. T. Lin, P.-T. Chou, *Tetrahedron,* **2010**, 66, 8629-8634.

[21] (a) I. Borges, Jr, E. Uhl, L. Modesto-Costa, A. J. A. Aquino, H. Lischka, *J. Phys. Chem. C*, **2016**, 21818-21826; (b) D. Jacquemin, A. Planchat, C. Adamo, B. Mennucci, *J. Chem. Theory. Comput.*, **2012**, 8, 2359-2372, (c) A. Monti, H. J. M. de Groot, F. Buda, *J. Phys. Chem. C*, **2014**, 118, 15600-15609, (d) Y. Tawada, T. Tsundea, S. Yanagisawa, T. Yanai, K. Hirao, *J. Chem. Phys.*, **2004**, 120, 8425-8433.

[22] R. Rybakiewicz, J. Zapala, D. Djurado, R. Nowakowski, P. Toman, J. Pfleger, J.-M. Verilhac, M. Zagorska, A. Pron, *Phys. Chem. Chem. Phys.* **2013**, 15, 1578-1587.

[23] S. K. Lee, Y. Zu, A. Herrmann, Y. Geerts, K. Müllen, A. J. Bard, *J. Am. Chem. Soc.* **1999**, 121, 3513-3530.

[24] A. Yassin, P. Leriche, J. Roncali, *Macromol. Rapid Commun.* **2010**, 31, 1467-1472.

[25] L. Dai, Y. Xue, L. Qu, H.-J. Choi, J.-B. Baek, *Chem. Rev.* **2015**, 115, 4823-4892.

[26] M. Jakešová, D. H. Apaydin, M. Sytnyk, K. Oppelt, W. Heiss, N. S. Sariciftci, E. D. Głowacki, *Adv. Funct. Mater.* **2016**, 26, 5248-5254.

[27] S. Yanagida, A. Kabumoto, K. Mizumoto, C. Pac, K. Yoshino, *J. Chem. Soc. Chem. Commun.* **1985**, 474-475.

[28] G. M. Suppes, P. J. Fortin, S. Holdcroft, *J. Electrochem. Soc.* **2015**, 162, H551.

[29] a) A. Yassin, G. Savitha, P. Leriche, P. Fre`re, J. Roncali, *New J. Chem.* **2012**, 36, 2412-2416;.b) R. Grisorio, G. Allegretta, G. P. Suranna, P. Mastrorilli, A. Loiudice, A. Rizzo, M. Mazzeo, G. Gigli, *J. Mat. Chem.* **2012**, 22, 19752-19760.

[30] a) F. Würthner, V. Stepanenko, Z. Chen, C. R. Saha-Moller, N. Kocher, D. Stalke, *J. Org. Chem.* **2004**, 69, 7933 - 7939; b) T. D. M. Bell, S. Yap, C. H. Jani, S. V. Bhosale, J. Hofkens, F. C. De Schryver, S. J. Langford, K. P. Ghiggino, *Chem. Asian J.* **2009**, 4, 1542 – 1550.

[31] a) C. Thalacker, C. Röger, F. Würthner, *J. Org. Chem.* **2006**, 71, 8098-8105; b) K. Sreenath, J. R. Allen, M. W. Davidson Lei Zhu, *Chem. Commun.* **2011**, 47, 11730-11732; c) S. Guo, W. Wu, H. Guo, J. Zhao, *J. Org. Chem.* **2012**, 77, 3933−3943.

[32] M. J. Frisch, G. W. Trucks, H. B. Schlegel, G. E. Scuseria, M. A. Robb, J. R. Cheeseman, G. Scalmani, V. Barone, B. Mennucci, G. A. Petersson, H. Nakatsuji, M. Caricato, X. Li, H. P. Hratchian, A. F. Izmaylov, J. Bloino, G. Zheng, J. L. Sonnenberg, M. Hada, M. Ehara K. Toyota, R. Fukuda, J. Hasegawa, M. Ishida, T. Nakajima, Y. Honda, O. Kitao, H. Nakai, T. Vreven, J. A. Montgomery, Jr., J. E. Peralta, F. Ogliaro, M. Bearpark, J. J. Heyd, E. Brothers, K. N. Kudin, V. N. Staroverov, T. Keith, R. Kobayashi, J. Normand, K. Raghavachari, A. Rendell, J. C. Burant, S. S. Iyengar, J. Tomasi, M. Cossi, N. Rega, J. M. Millam, M. Klene, J. E. Knox, J. B. Cross, V. Bakken, C. Adamo, J. Jaramillo, R. Gomperts, R. E. Stratmann, O. Yazyev, A. J. Austin, R. Cammi, C. Pomelli, J. W. Ochterski, R. L. Martin, K. Morokuma, V. G. Zakrzewski, G. A. Voth, P. Salvador, S. Dannenberg, A. D. Dapprich, O. Daniels, J. B. Farkas, J. V. Foresman, J. Ortiz, J. Cioslowski, D. J. Fox, Gaussian 09, Revision D.01, Gaussian, Inc., Wallingford CT, **2013**.

[33] a) A. D. Becke, *J. Chem. Phys.* **1993**, 98, 1372-1377; b) A. D. Becke, *J. Chem. Phys.* **1993**, 98, 5648-5652; c) C. T. Lee, W. T. Yang, R. G. Parr, *Phys. Rev. B* **1988**, 37, 785.

[34] J. Tomasi, B. Mennucci, R. Cammi, *Chem. Rev.* **2005**, 105, 2999-3094.

[35] a) R. Bauernschmitt, R. Ahlrichs, *Chem. Phys. Lett.* **1996**, 254, 454-464; b) M. E. Casida, C. Jamorski, K. C. Casida, D. R. Salahub, *J. Chem. Phys.* **1998**, 108, 4439-4449; c) R. E. Stratmann, G. E. Scuseria, M. J. Frisch, *J. Chem. Phys.* **1998**, 109, 8218-8224; d) C. V. Caillie, R. D. Amos, *Chem. Phys. Lett.* **1999**, 308, 249-255; e) C. V. Caillie, R. D. Amos, *Chem. Phys. Lett.* **2000**, 317, 159; f) F. Furche, R. Ahlrichs, *J. Chem. Phys.* **2002**, 117, 7433-7447; g) G. Scalmani, M. J. Frisch, B. Mennucci, J. Tomasi, R. Cammi, V. Barone, *J. Chem. Phys.* **2006**, 124, 1-7.

[36] N. M. O'Boyle, A. L. Tenderholt, K. M. Langner, *J. Comput. Chem.* **2008**, 29, 839-845.

[37] R. L. Martin, *J. Chem. Phys.* **2003**, 118, 4775-4777.

[38] R. Dennington, T. Keiyh, J. Millam, *GaussView*, Version 5, *Semichem Inc.,* Shawnee Mission, KS, **2009**.

FULL PAPER

Low and high molecular mass dithienopyrrole-naphthalene bisimide donor-acceptor compounds: synthesis, electrochemical and spectroelectrochemical behaviour

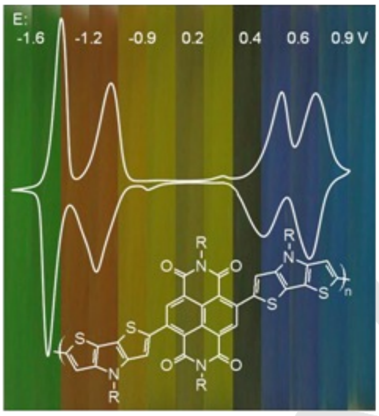

*Author(s), Corresponding Author(s)**
Renata Rybakiewicz, Eric D. Glowacki*, Lukasz Skorka, Sandra Pluczyk, Pawel Zassowski, Dogukan Hazar Apaydin, Mieczyslaw Lapkowski, Malgorzata Zagorska, Adam Pron**

Page No. – Page No.

Title